Research Article | Vol. 27, No. 22 / 28 October 2019 / Optics Express 32630
Optics EXPRESS

High-harmonic generation in solids driven by counter-propagating pulses

A. Korobenko,[1,2,*] T. J. Hammond,[3] C. Zhang,[1,2] A. Yu. Naumov,[1] D. M. Villeneuve,[1] and P. B. Corkum[1,2]

[1] *Joint Attosecond Science Laboratory, National Research Council of Canada and University of Ottawa, 100 Sussex Dr, Ottawa, ON K1A 0R6, Canada*
[2] *Department of Physics, University of Ottawa, 25 Templeton St, Ottawa, ON K1N 6N5, Canada*
[3] *Department of Physics, University of Windsor, 401 Sunset Ave Windsor, ON N9B 3P4, Canada*
[*] *akoroben@uottawa.ca*

Abstract: We used two 800 nm laser pulses propagating in the opposite directions, to drive the emission of high-order vacuum ultra-violet harmonics off of the surface of an MgO (100) single crystal. We demonstrated the advantages that our approach provides compared to a single beam geometry, in both forward and backward emission.

1. Introduction

Intense light can drive non-linear currents in bulk of solids, leading to emission of high-order harmonics (HHG) [1–6]. In the case of wide-bandgap dielectrics these harmonics can stretch to the vacuum ultraviolet (VUV) [3], suggesting their use as a prospective VUV source.

High harmonics from solids are often generated by passing a focused laser beam through a crystal and detecting the emitted radiation along the direction of propagation, hereafter referred to as forward emission [7]. Since the VUV absorption length of many wide-bandgap crystals is tens of nanometers [8], only a thin layer of material, close to the output interface, contributes to the high harmonics [9]. Using crystals thicker than a few tens of nanometers does not improve the generation efficiency. On the contrary, long crystals can be deleterious.

Efficient high-harmonics generation in wide-bandgap materials requires peak intensities of $\gtrsim$10 TW/cm^2. Propagation in even a thin sample on substrate can severely modify a high intensity fundamental pulse. For example, the 200 μm-thick crystal of MgO used in this work has a non-linear index of refraction of $n_2 = 8.1\times10^{-4}$cm^2/TW [10]. A Gaussian pulse of peak intensity of 5 TW/cm^2 passing through such a crystal would accumulate a B-integral $B = \frac{2\pi}{\lambda}\int n_2 I dz \sim 2\pi$. Here I is the pulse intensity, λ its wavelength, and B characterizes the phase variation across the beam profile that the pulse would acquire after the propagation. This phase modification is transferred to the phase of the generated harmonics [1], leading to a deterioration of the spatial properties of the emitted radiation.

Recently a different approach was demonstrated, where harmonic emission was detected in the specular direction with respect to the driving beam [7]. This approach, called backward emission, does not require a laser pulse to propagate through the bulk of the solid prior to generation. Therefore, higher intensities can be used in thick crystals, without inducing any phase distortion onto the laser field. However, since the fundamental and VUV beams propagate in the opposite directions, phase mismatch accumulates over the distance of less than a single VUV wavelength, substantially impacting the efficiency of generation.

In this work we explore a combination of the two approaches discussed above. Two counter-propagating laser pulses of the same wavelength simultaneously form a (partial or full) standing wave with a field anti-node inside the material near its back interface. This scheme provides two benefits. First, the same peak intensity is achieved at a substantially lower power of transmitted laser beam, decreasing the propagation effects (two counter propagating fields of equal intensity,

#375402 https://doi.org/10.1364/OE.27.032630
Journal © 2019 Received 15 Aug 2019; revised 1 Oct 2019; accepted 2 Oct 2019; published 24 Oct 2019

Optics EXPRESS

I_0, add up to the same peak field strength as a single beam of intensity $4I_0$). Second, compared to a purely backward emission geometry, the approach benefits from improved phase matching, as discussed later.

2. Experimental setup

We spectrally broadened an output of a 1 kHz repetition rate 27 fs Ti:Sapphire laser in a Ne-filled hollow-core fiber and compressed it by a set of chirped mirrors to a FWHM duration of 7.0 fs, centered at 775 nm. We picked 8% of the beam (E_1) by a fused silica window and passed through a piezo-controlled delay stage to be used in a forward emission geometry. We attenuated the rest of the beam (E_2) with a broadband half-wave plate followed by a wire-grid polarizer, and used it as a driver for backwards-emitted harmonics. The energies of the first and the second laser pulses were 4 μJ and 0-50 μJ respectively, prior to entering the vacuum section of the system (Fig. 1).

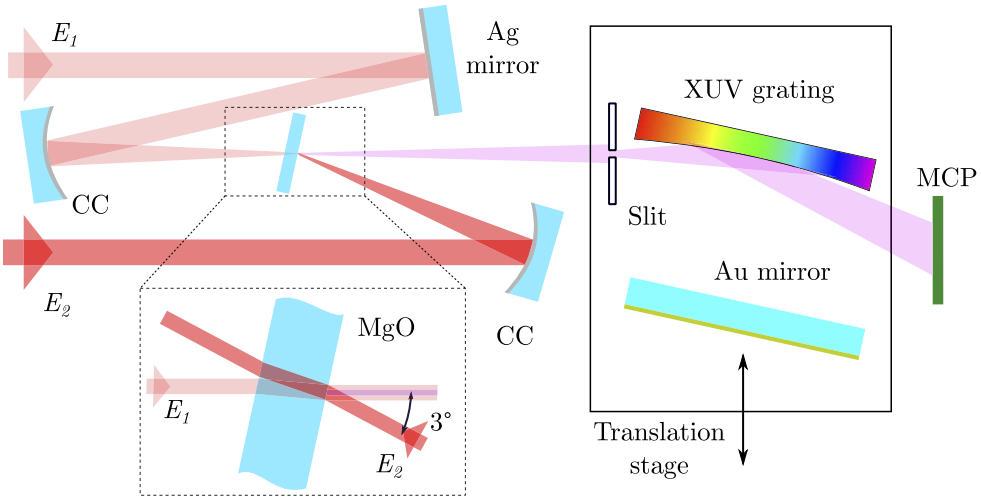

Fig. 1. Vacuum section of the experimental setup. Two laser beams (E_1 and E_2) were focused with protected silver concave mirrors (CC, 1 m radius of curvature) onto a back surface of MgO sample at a nearly straight angle of 177° to each other. HHG radiation emitted from this surface hit a slit of an XUV spectrometer followed by a curved XUV grating dispersing the beam over a microchannel plate XUV detector (MCP). The slit and the grating were mounted on a motorized platform allowing to replace them with a grazing incidence gold mirror and to observe energy unresolved far-field profile of the HHG.

A residual pressure of $\lesssim 10^{-6}$ mbar along the beam path prevented strong absorption of the generated radiation. Inside the vacuum chamber two identical concave protected silver mirrors (CC) with a radius of curvature of 1000 mm, focus the beams onto the same spot of a back surface of a two-side polished 200 μm-thick (100)-cut magnesium oxide (MgO) sample. We measured the waist of the beams with a knife edge to be (140 ± 5) μm FWHM. We intersected the beams in a nearly anti-parallel configuration, at an angle of $180° - 3° = 177°$, with the forward propagating field passing through the crystal. Keeping this angle small simplified spatio-temporal overlap of the beams. It also reduced the analytical treatment to a single dimension.

We oriented the surface of the sample in a way that the forward-propagating beam coincided with the specular Fresnel reflection of the backward-propagating beam. Under these conditions, the wave vectors $\mathbf{k_1}$ and $\mathbf{k_2}$ of the two beams inside the crystal were the mirror images of each other with respect to the sample surface, and only differed by a vector parallel to the normal to the latter, $\mathbf{n}$: $\mathbf{k_1} - \mathbf{k_2} = 2(\mathbf{k_1} \cdot \mathbf{n})\mathbf{n}$. The spatial phases of the two beams, $\varphi_1(\mathbf{r}) = \mathbf{k_1} \cdot \mathbf{r}$ and

Optics EXPRESS

$\varphi_2(\mathbf{r}) = \mathbf{k_2} \cdot \mathbf{r}$ at the position $\mathbf{r}$, therefore satisfied $\varphi_1(\mathbf{r}) - \varphi_2(\mathbf{r}) = (\mathbf{k_1} - \mathbf{k_2}) \cdot \mathbf{r} = 2(\mathbf{k_1} \cdot \mathbf{n})(\mathbf{n} \cdot \mathbf{r})$. The last expression suggests that the phase difference between the two waves is the same at all positions satisfying $(\mathbf{n} \cdot \mathbf{r}) = const$, i.e. inside any plane parallel to the crystal interface. Equivalently, the planes of the nodes (and anti-nodes) of the resulting standing wave are parallel to the crystal surface.

High harmonics generated from the back surface of MgO passed through a 300 μm slit of the extreme ultraviolet (XUV) spectrometer followed by a 300 grooves/mm laminar-type XUV diffraction grating and an imaging MCP detector. The XUV grating mapped the photon energy to the horizontal spatial coordinate on the detector, while the vertical was preserved for the beam profile. We captured the image formed on the MCP by the harmonic radiation with a CCD camera, sitting outside of the chamber next to a viewport. The camera exposure was set to 50-200 ms depending on the signal intensity, which corresponded to 50-200 laser shots. We mounted the slit and grating on a linear translation stage, allowing them to be exchanged with a gold mirror at a grazing angle. With the gold mirror in place, we could image the VUV beam profile directly with an MCP detector and CCD camera.

3. Results and discussion

To begin we fixed the peak intensities of both beams to the same value of (1.66 ± 0.09) TW/cm^2 and moved the gold mirror into the beam path. Figure 2 shows the measured VUV profiles, generated with forward-propagating (Fig. 2(a)) and backward-propagating field alone (Fig. 2(b), amplified 10 times). The HHG signal observed in the case of forward emission was almost 20 times higher in magnitude, and also demonstrated higher beam divergence of 3.7 mrad against 2.2 mrad FWHM in case of backward emission.

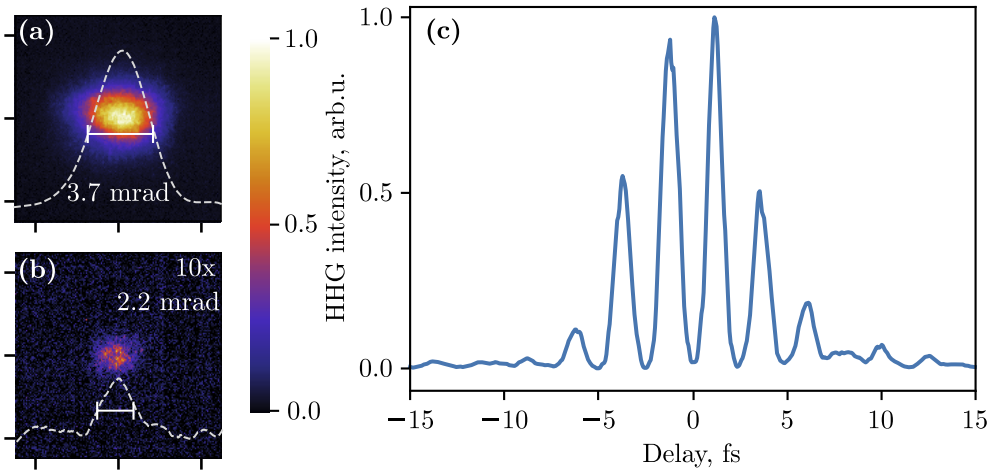

Fig. 2. HHG beam profiles, obtained with the XUV grating removed from the beam path in (a) forward and (b) backward emission geometries, taken at the same laser peak intensity of $I_{\text{peak}} = 1.66$ TW/cm^2. Large phase mismatch between the fundamental and the HHG resulted in a strong decrease in the harmonic brightness in the backward emission configuration, while the non-linear phase accumulated by the laser beam during its propagation through the 200 μm MgO crystal resulted in a higher beam divergence in the forward emission geometry. (c) Total harmonic yield with the both beams present, as a function of the relative delay between them.

Higher beam divergence of the forward emission is expected due to the Kerr effect in the bulk of the crystal, imposing spatial-dependent phase on the laser beam. Increasing the peak intensity

Optics EXPRESS

above 1.66 TW/cm^2, which corresponds to peak electric field amplitude of (0.269 ± 0.007) V/Å inside the crystal and the B-integral B = 2.2 rad, increased the total harmonics intensity, and also lead to further increase of beam divergence.

Two factors contribute to a much higher VUV fluence observed in the forward direction. First, since in this case the driving field and the generated harmonics propagate in the same direction inside the material, there is a smaller phase mismatch accumulated along the propagation path, compared to the backward emission when they travel in the opposite directions [7]. The second factor is due to the Fresnel reflection of the fundamental laser beam from the crystal surface, which increases the electric field. MgO has index of refraction of $n(\lambda = 775\ \text{nm}) = 1.7284$ [11], corresponding to an amplitude reflection coefficient $r = 0.27$ (the intensity reflection coefficient $R = r^2 = 0.071$) for medium-to-vacuum transmission. Positive sign of the amplitude causes constructive interference of the electric fields at the interface, resulting in a peak value of 0.269 V/Å × 1.27 = 0.341 V/Å. This value is equal to the amplitude of single traveling wave with peak intensity of 2.67 TW/cm^2 (approximately 1.61 times higher than the input beam).

With both beams present, we measured the total HHG intensity, integrated over the beam profile, as a function of the relative delay between the pulses. The result is plotted in Fig. 2(c). Strong, nearly two order of magnitude deep, signal oscillations were observed. They occurred when the pulses temporally overlapped on the surface, as the surface was passing nodes and anti-nodes of the electric field of the standing wave. The observed period of 2.5 fs corresponded to the period of a fundamental laser field oscillations.

To compare the efficiency of HHG in counter-propagating and backward emission configurations in details, we performed spectrally-resolved measurements using the total field of the same peak amplitude. With the XUV grating and slit in place we repeated the time dependent measurements.

To carry out this comparison over a broader spectral range, we increased the peak intensity of the backward propagating pulse to (11.9 ± 0.6) TW/cm^2 to extend the harmonic cut-off. The intensity of the forward propagating pulse was kept at 1.66 TW/cm^2 to avoid any stronger distortion of the fundamental. We recorded a set of images at different delays. At the delays corresponding to the temporal overlap of the pulses at the surface, strong modulation of the integrated VUV yield was accompanied by the oscillations in the harmonics cut-off energy. The latter reached its maxima together with the total yield, when the pulses coherently interfered at the surface. We then selected the image corresponding to the highest signal, when the two pulses were best overlapped and analyzed it (Fig. 3(a)). We estimated the amplitudes of the forward and backward propagating fields to be 0.269 V/Å and 0.79 V/Å respectively, adding up to a total amplitude of (1.06 ± 0.02) V/Å. This estimate included the Fresnel reflection discussed above.

We captured another image in a purely backward emission geometry with the peak field intensity of (25.5 ± 1.4) TW/cm^2. This image corresponding to the total peak field amplitude of (1.05 ± 0.03) V/Å (same as in the counter-propagating setup), is shown in Fig. 3(b), scaled by a factor of 2. Both spectra demonstrate a similar harmonic cut-off, with harmonics H5 through H17 observed. The brightness of the lowest observed harmonics H5 and H7 is underestimated due to the decreased efficiency of the XUV grating below 15 eV. The harmonics above 20 eV (H13 and higher) are generated by interband transitions involving a higher-lying conduction band of MgO [12], resulting in a characteristic step in signal brightness at 20 eV.

Figures 3(c) and 3(d) show the comparison of energy-integrated far-field beam profiles for counter-propagating (red) and backward-emission configurations, for harmonics H9 and H15 respectively. Both harmonics demonstrate an increase in the beam divergence (1.7 mrad vs 1.3 mrad for H9, 1.4 mrad vs 0.9 mrad for H15) and higher total intensity (3 times for H9, 4 times for H11) in counter-propagating configuration. We observed similar effects for other harmonics. Note the difference divergence between the backward emission and counter-propagating setups. It can be attributed to the additional accumulated nonlinear phase in the forward-propagating beam. In addition the beam divergence for both counter-propagating and backward emission

Optics EXPRESS

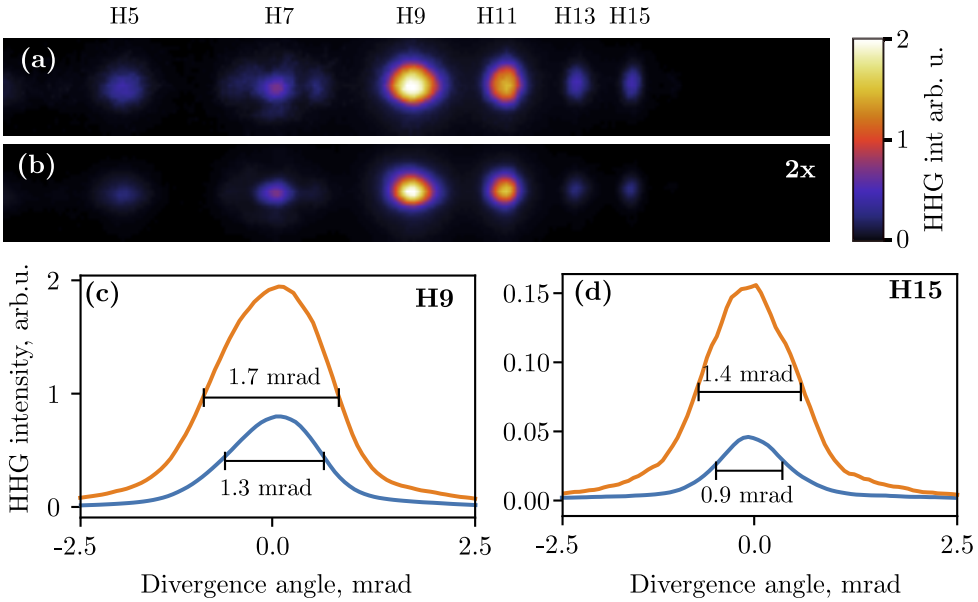

Fig. 3. (a, b) Raw images from the detector of the XUV spectrometer, taken with (a) two counter-propagating pulses of the field intensities of $I_1 = 1.66$ TW/cm^2 and $I_2 = 11.9$ TW/cm^2 and (b) a single backward-propagating beam with a peak intensity of $I_2 = 25.5$ TW/cm^2. In both cases the peak field amplitude was 1.06 V/Å near the interface. (c, d) Far-field profile comparison between backward only (blue) and counter-propagating (red) geometry at optimal two pulse delay of harmonics orders (c) H9 and (d) H15. Peak intensities are the same as in (a, b). Horizontal bars indicate FWHM of the beams.

geometries were lower compared to the spectrally-integrated measurements on Fig. 2(a)–2(b). This can be attributed to the perturbative intensity scaling at lower fields, resulting in narrower waist of the generated harmonics, and leading to their higher divergence due to diffraction. A quantitative analysis of phase matching as a source of intensity increase is provided below.

Consider two monochromatic plane waves of the same radial frequency ω and linear polarization, propagating along the x-axis in opposite directions. The material has refractive index n at this frequency and occupies $x<0$ half-space. The total electric field can be written as:

$$E(t,x) = E_1(t,x) + E_2(t,x) = E_1^0 e^{i\omega\frac{n}{c}x - i\omega t} + E_2^0 e^{-i\omega\frac{n}{c}x - i\omega t} = E^0(x)e^{i\varphi(x)}e^{-i\omega t},$$

where $E_{1,2}^0$ are the amplitudes of the waves propagating in the positive and negative x directions respectively, c is the speed of light in vacuum, $E^0(x) = \sqrt{E_1^{0^2} + E_2^{0^2} + 2E_1^0 E_2^0 \cos\frac{2\omega n x}{c}}$, and $\varphi(x) = \arctan\left(\frac{E_1^0 - E_2^0}{E_1^0 + E_2^0}\tan\frac{\omega n x}{c}\right)$.

This field can generate high harmonics anywhere in the crystal at $x<0$. However, the VUV radiation produced deep inside the solid will be absorbed before reaching the vacuum at $x>0$ where it can freely propagate. Therefore, only a layer $|x|<\delta$, where δ is the propagation length, is important in generation of HHG. In what follows it is assumed that

$$\delta \ll \lambda = 2\pi c/\omega n, \tag{1}$$

which is commonly observed in crystals. For example, the band gap of MgO is 7.8 eV [13], leading to strong absorption of the VUV radiation in the studied energy range from 8 to 25 eV. Comparing δ, varying between 10 and 20 nm in this energy range [14], to a fundamental wavelength inside

Optics EXPRESS

the material $\lambda = 775$ nm$/n = 448$ nm, we can verify the inequality (1) to be satisfied under the used experimental conditions. Under this assumption in the context of high-harmonics generation we are only interested in a fundamental field structure at $|x| \ll 2\pi c/\omega n$, $x<0$. In this case the above expressions $E^0(x)$ and $\varphi(x)$ can be expanded in powers of $\frac{\omega n x}{c}$. Keeping only first order, one arrives at:

$$E(t,x) \approx (E_1^0 + E_2^0)e^{i\omega\frac{n_{\text{eff}}}{c}x - i\omega t}, \tag{2}$$

with $n_{\text{eff}} = n\frac{E_1^0 - E_2^0}{E_1^0 + E_2^0}$. This expression implies that for the purpose of high-harmonic generation the fundamental field is equivalent to a plane wave, propagating in an effective medium with index of refraction $|n_{\text{eff}}|$ along the direction $\text{sgn}(n_{\text{eff}})\hat{x}$.

The efficiency of harmonic generation of order ν is then reduced to the integration of the phase mismatch factor $e^{i\Delta k x}$ along the generation medium [15]. Here, $\Delta k = \nu k_{\text{eff}} - k_\nu$ is the phase mismatch, $k_{\text{eff}} = \omega\frac{n_{\text{eff}}}{c}$ and $k_\nu = \nu\omega\frac{\underline{n}(\nu\omega)}{c}$ are the wavenumbers of the fundamental field and its ν-th harmonic respectively, and $\underline{n}(\nu\omega) = n(\nu\omega) + i\kappa(\nu\omega)$ is the VUV complex index of refraction. The total field of the ν-th harmonic at the surface (neglecting the VUV reflection at the interface), will have contributions from planar emitters at all possible planes $x = x'$, $x'<0$. Each emitter is driven by the fundamental with the same amplitude $E_1^0 + E_2^0$, and phase $\omega\frac{n_{\text{eff}}}{c}x'$. Therefore, each one emits radiation of amplitude $E_\nu dx'$, and phase $\nu\omega\frac{n_{\text{eff}}}{c}x'$, where dx' is the layer thickness. The resulting plane wave, originating from $x = x'$ plane and moving in the $+\hat{x}$ direction, therefore takes form

$$\mathrm{d}E_\nu(x',x,t) = E_\nu e^{i\nu\omega\frac{n_{\text{eff}}}{c}x'} e^{i\nu\omega\frac{\underline{n}(\nu\omega)}{c}(x-x')}\mathrm{d}x'.$$

To get the total intensity of the ν-th harmonic at the surface $x = 0$ we integrate over all emitters $x'<0$, and take the square of the absolute value of the acquired amplitude:

$$\begin{aligned} I_\nu &\propto \left|\int_{-\infty}^{0} \mathrm{d}x'\; e^{i\nu\omega\frac{n_{\text{eff}}}{c}x'} e^{-i\nu\omega\frac{n(\nu\omega)+i\kappa(\nu\omega)}{c}x'}\right|^2 \\ &= \frac{c^2/(\omega\nu)^2}{(n_{\text{eff}} - n(\omega\nu))^2 + \kappa(\omega\nu)^2} \end{aligned} \tag{3}$$

Two factors in the denominator can be identified to contribute to the generation efficiency independently. The first, $(n_{\text{eff}} - n(\omega\nu))^2$, corresponds to the phase mismatch; while the second, $\kappa(\omega\nu)^2$, to the absorption of harmonics. It is worth noting that in the whole range of observed VUV emission from 5 to 30 eV, the phase mismatch is a largely dominating effect in the case of backward emission with the absorption contributing no more than 20% to overall efficiency. This is part of the reason the forward emission was more efficient in Fig. 2(a)–2(b). An interesting implication follows from the expression (3) at very high XUV photon energies, when the real part of the refractive index in many crystals approaches unity, $n(\omega\nu) \sim 1$ [8]. Phase-matching condition $n_{\text{eff}} - 1 = 0$ in this case is achieved for $E_2^0 = E_1^0\frac{n-1}{n+1}$, satisfied for a Fresnel reflection of a single forward-propagating beam from the crystal surface.

Using expression (3) and MgO optical constants from [14] we calculate the expected increase in VUV intensity that the counter-propagating configuration provides relative to the backwards emission only. For the field amplitudes of 0.27 V/Å + 0.79 V/Å = 1.06 V/Å, used in Fig. 3, this increase is given by the expression $\frac{(n+n(\omega\nu))^2+\kappa(\omega\nu)^2}{(0.49n+n(\omega\nu))^2+\kappa(\omega\nu)^2}$ and is plotted in Fig. 4(b) as a function of photon energy with a black dashed line. The characteristic step at ~20 eV, present in both the calculations and measurements, is due to the specific shape of the refractive index of MgO. While simple phase matching calculations seem to reflect the general shape of the measured dependence, they predict values 40% lower than the observed ones.

Optics EXPRESS

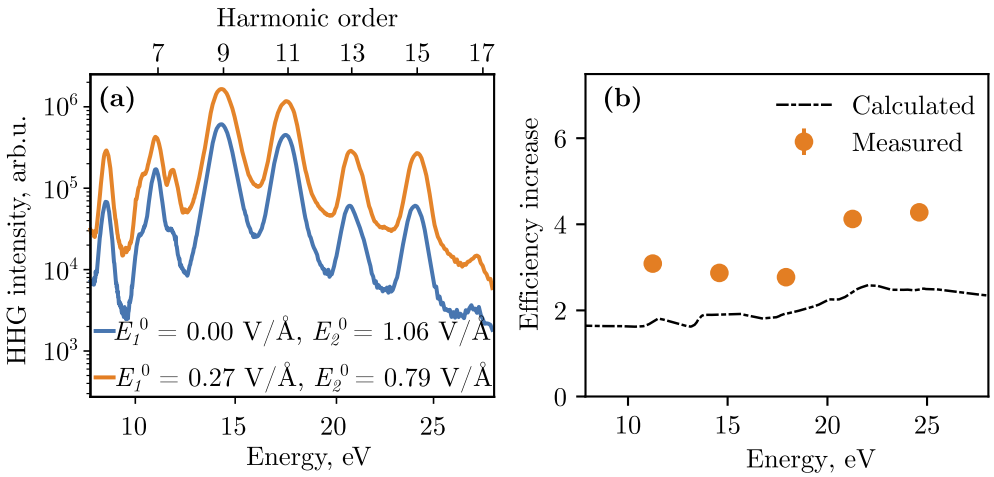

Fig. 4. (a) Comparison of the HH spectra generated with a single pulse of I_{peak} = 25.5 TW/cm^2 in a backward emission geometry (blue) and two counter-propagating pulses $I^{\text{tr}}_{\text{peak}}$ = 1.66 TW/cm^2, $I^{\text{r}}_{\text{refl}}$ = 11.9 TW/cm^2 (red). Both curves correspond to the same peak field strength of 1.06 V/Å at the interface. The signal intensity observed in the two pulse case is approximately 3 to 4 times higher. (b) Calculated (black dashed line) and observed (red circles) HHG efficiency increase in the counter-propagating geometry relative to the backward emission geometry, at the same peak field of 1.06 V/Å at the interface.

4. Conclusion

In conclusion, we implemented a new approach to high-harmonic generation in solids combining forward and backward propagating pulses. This approach allows to simultaneously keep the peak field amplitude high, which is necessary for generation of XUV harmonics; and at the same time does not suffer from propagation effects, which are intrinsic to a purely forward emission generation. Compared to a backward emission geometry this approach required a lower total pulse energy while still being more efficient due to improved phase matching. We applied this technique to MgO crystal to show a 3 to 4-fold increase in the harmonics intensity in the 10 to 25 eV energy range at half the total driving laser power. The observed intensity increase was higher than predicted by phase matching considerations. The origin of this discrepancy is not yet clear. One possible reason is the higher sample temperature in case of the backward emission, caused by the twofold increase in the average laser power. High temperature has previously been observed to be detrimental to the high harmonic generation in solids [16].

Funding

Air Force Office of Scientific Research (FA9550-16-1-0109); Canada Research Chairs; Natural Sciences and Engineering Research Council of Canada; National Research Council, Joint Center for Extreme Photonics.

Acknowledgments

We thank David Crane and Ryan Kroeker for their technical support.

Disclosures

The authors declare no conflicts of interest.

Optics EXPRESS

References

1. S. Ghimire, A. D. Dichiara, E. Sistrunk, P. Agostini, L. F. Dimauro, and D. A. Reis, "Observation of high-order harmonic generation in a bulk crystal," Nat. Phys. **7**(2), 138–141 (2011).
2. O. Schubert, M. Hohenleutner, F. Langer, B. Urbanek, C. Lange, U. Huttner, D. Golde, T. Meier, M. Kira, S. W. Koch, and R. Huber, "Sub-cycle control of terahertz high-harmonic generation by dynamical Bloch oscillations," Nat. Photonics **8**(2), 119–123 (2014).
3. T. T. Luu, M. Garg, S. Yu. Kruchinin, A. Moulet, M. T. Hassan, and E. Goulielmakis, "Extreme ultraviolet high-harmonic spectroscopy of solids," Nature **521**(7553), 498–502 (2015).
4. G. Vampa, T. J. Hammond, N. Thiré, B. E. Schmidt, F. Légaré, C. R. McDonald, T. Brabec, and P. B. Corkum, "Linking high harmonics from gases and solids," Nature **522**(7557), 462–464 (2015).
5. Y. S. You, D. A. Reis, and S. Ghimire, "Anisotropic high-harmonic generation in bulk crystals," Nat. Phys. **13**(4), 345–349 (2017).
6. M. Sivis, M. Taucer, G. Vampa, K. Johnston, A. Staudte, A. Y. Naumov, D. M. Villeneuve, C. Ropers, and P. B. Corkum, "Tailored semiconductors for high-harmonic optoelectronics," Science **357**(6348), 303–306 (2017).
7. G. Vampa, Y. S. You, H. Liu, S. Ghimire, and D. A. Reis, "Observation of backward high-harmonic emission from solids," Opt. Express **26**(9), 12210 (2018).
8. http://henke.lbl.gov/optical_constants/filter2.html
9. S. Ghimire, A. D. Dichiara, E. Sistrunk, G. Ndabashimiye, U. B. Szafruga, A. Mohammad, P. Agostini, L. F. Dimauro, and D. A. Reis, "Generation and propagation of high-order harmonics in crystals," Phys. Rev. A **85**(4), 043836 (2012).
10. R. Adair, L. L. Chase, and S. A. Payne, "Nonlinear refractive index of optical crystals," Phys. Rev. B **39**(5), 3337–3350 (1989).
11. R. Stephens and I. Malitson, "Index of refraction of magnesium oxide," J. Res. Natl. Bur. Stand. **49**(4), 249 (1952).
12. Y. S. You, M. Wu, Y. Yin, A. Chew, X. Ren, S. Gholam-Mirzaei, D. A. Browne, M. Chini, Z. Chang, K. J. Schafer, M. B. Gaarde, and S. Ghimire, "Laser waveform control of extreme ultraviolet high harmonics from solids," Opt. Lett. **42**(9), 1816 (2017).
13. D. M. Roessler and W. C. Walker, "Electronic Spectrum and Ultraviolet Optical Properties of Crystalline MgO," Phys. Rev. **159**(3), 733–738 (1967).
14. D. M. Roessler and W. C. Walker, "Optical Constants of Magnesium Oxide and Lithium Fluoride in the Far Ultraviolet," J. Opt. Soc. Am. **57**(6), 835 (1967).
15. R. W. Boyd, *Nonlinear Optics* (Academic, 2008), 3rd ed.
16. K. F. Lee, X. Ding, T. J. Hammond, M. E. Fermann, G. Vampa, and P. B. Corkum, "Harmonic generation in solids with direct fiber laser pumping," Opt. Lett. **42**(6), 1113–1116 (2017).